Available online at www.sciencedirect.com
SCIENCE DIRECT®
Journal of Magnetism and Magnetic Materials 302 (2006) 237–243
Journal of magnetism and magnetic materials
www.elsevier.com/locate/jmmm

Spin dynamics and magnon–phonon interactions in $Nd_{0.6}Sr_{0.4}MnO_3$

B.J. Kirby[a,*], J.J. Rhyne[a,b], H. Kaiser[c], H. Kuwahara[d], Y. Tokura[e,f,g]

[a]*Department of Physics and Astronomy, University of Missouri, Columbia, MO 65211, USA*
[b]*Lujan Neutron Scattering Center, Los Alamos National Laboratory, Los Alamos, NM 87545, USA*
[c]*Indiana University Cyclotron Facility, Bloomington, IN 47405, USA*
[d]*Department of Physics, Sophia University, Tokyo 102-8554, Japan*
[e]*Department of Applied Physics, University of Tokyo, Tokyo 113-8656, Japan*
[f]*Correlated Electron Research Center, National Institute of Advanced Industrial Science and Technology, Tsukuba 305-0046, Japan*
[g]*Spin Superstructure Project, Exploratory Research for Advaced Technology, Japan Science and Technology Corporation, Tsukuba 305-8562, Japan*

Received 1 June 2005; received in revised form 25 August 2005
Available online 3 October 2005

Abstract

The magnon dispersion of $Nd_{0.60}Sr_{0.4}MnO_3$ has been measured along the $[q\,q\,q]$, $[q\,q\,0]$, and $[0\,0\,q]$ propagation directions using inelastic neutron scattering. Modes attributed to both Mn–Mn interactions and Nd–Mn interactions were detected. At low temperatures, and for all three directions, the low q Mn–Mn dispersion closely followed a Heisenberg nearest-neighbor model calculation, before showing marked softening at higher values of q. For the $[q\,q\,0]$ and $[0\,0\,q]$ directions, this softening appears to correspond with intersection with 20 and 40 meV phonon branches, respectively. At low temperatures, and for all three directions, the Nd–Mn dispersion followed the calculated Heisenberg dispersion for all measured points. Additionally, the temperature dependence of the magnon stiffness parameter D was measured up to $T_C = 273\,K$, and showed conventional temperature renormalization behavior.

PACS: 63.00.00; 75.30.00; 75.47.Lx

Keywords: CMR; Manganite; Neutron scattering

1. Introduction

The perovskite manganites have been the subject of intense research in the last decade, following the discovery of the colossal magnetoresistive (CMR) effect in specific perovskite compounds of the formula $A_{1-x}B_xMnO_3$ (where the A and the B are trivalent and divalent ions, respectively) [1,2]. The CMR effect in these materials results from an applied magnetic field driving a phase transition from an insulating paramagnet to a spin-aligned metal. Which phase is stable in a magnetic field is determined by competition between two processes: Zener double exchange [3–5], which delocalizes valence electrons, and the Jahn–Teller effect [6], which localizes valence electrons. Double exchange can dominate if the core Mn spins are well aligned, and conversely the Jahn–Teller effect dominates when the spins are disordered. If a CMR system is in the high-temperature paramagnetic phase, it is dominated by the Jahn–Teller effect, and has localized valence electrons. By aligning the core spins with a large magnetic field, the balance swings in favor of double exchange, and the valence electrons become less localized, drastically lowering the electrical resistance. This is the nature of the CMR effect.

Manifestations of Jahn–Teller electron-lattice coupling (polarons) have been seen in the Debye parameters and the MnO_6 octahedra bond lengths measured with neutron diffraction [7–9]. Additional evidence of Jahn–Teller polarons has been provided by neutron diffuse scattering [10,11] and measurement of Jahn–Teller phonon damping using inelastic neutron scattering [12].

The first full-zone measurement of the magnon dispersion in a Pb manganite ($La_{0.7}Pb_{0.3}MnO_3$) by Perring et al.

*Corresponding author. Tel.: (505) 6670628; fax: (505) 6652676.
E-mail address: bkirby@lanl.gov (B.J. Kirby).

0304-8853/$ - see front matter © 2005 Elsevier B.V. All rights reserved.
doi:10.1016/j.jmmm.2005.09.012

[13] was well represented by a conventional Heisenberg exchange model with only nearest-neighbor coupling of the form

$$\hbar\omega(q) = \Delta + 4J_1S(3 - \cos q_x a_0 - \cos q_y a_0 - \cos q_z a_0), \quad (1)$$

where q is the magnon wave vector, Δ is the energy gap at $q = 0$, J_1 is the nearest-neighbor exchange constant, and a_0 is the (cubic) lattice parameter. At small values of q this reduces to the familiar quadratic form

$$\hbar\omega(q) = \Delta + Dq^2, \quad (2)$$

where D is the magnon stiffness parameter that typically exhibits a temperature dependence

$$D(T) \approx D(0)\left[1 + \left(\frac{T}{T_C}\right)^{5/2}\right] \quad (3)$$

at low T, and a power-law form

$$D(T) \approx D(0)\left|\left(\frac{T}{T_C}\right) - 1\right|^{\nu-\beta}, \quad (4)$$

on approach to T_C with critical exponents $(\nu - \beta) = 0.34$ for a Heisenberg ferromagnet.

Although the conventional Heisenberg model explained the Pb-manganite magnon measurements, studies of other manganite materials have shown marked departures from nearest-neighbor Heisenberg behavior. In particular, single crystal results on $La_{0.7}Sr_{0.3}MnO_3$ [14], $Pr_{0.63}Sr_{0.37}MnO_3$ [15,16], $Nd_{0.7}Sr_{0.3}MnO_3$ [15,17], and the present work all show significant softening of the mode energies at the larger q values from that predicted by the Heisenberg fit. Dai et al. [17] showed that the magnon softening for $Nd_{0.7}Sr_{0.3}MnO_3$, $La_{0.7}Ca_{0.3}MnO_3$, and $Pr_{0.63}Sr_{0.37}MnO_3$ in the $[0\,0\,q]$ direction corresponds to the intersection of that mode with an optical phonon mode located around 20 meV, and that the magnon softening for $La_{0.7}Ca_{0.3}MnO_3$ and $Pr_{0.63}Sr_{0.37}MnO_3$ in the $[q\,q\,0]$ direction corresponds to the intersection of that mode with an optical phonon mode located around 40 meV. Woods [18] has presented a model for the magnon–phonon interaction in three-dimensional cubic ferromagnetic systems that predicts softening of the magnon mode that is consistent with the above cited, and present experimental results. Furthermore, Kaplan and Mahanti [19] have presented a one-dimensional double-exchange model, which predicts significant magnon softening at the zone boundary.

In addition to mode softening, the manganites show anomalies in the values of $D(0)/kT_C$. For most materials, $D(0)$ scales with T_C such that this ratio remains constant. In contrast (as pointed out by Fernandez-Baca et al. [15]), most manganites retain a nearly constant value of $D(0)$ (approximately 140–160 meV Å^{-2}) despite the fact that T_C can vary by nearly a factor of two.

2. Results

The present work on $Nd_{0.6}Sr_{0.4}MnO_3$ expands upon and adds corrections to the work presented by this group [20], in which optical phonon modes and other inelastic scattering were likely misidentified as magnons at high q. The $x = 0.4$ composition of $Nd_{1-x}Sr_xMnO_3$ is a ferromagnetic metal, somewhat above the optimal CMR composition of $x = 0.33$ (in contrast, the $NdSrMnO_3$ samples studied in Refs. [15,17] were slightly *below* the optimal CMR composition). The crystal used was grown by the floating zone technique and was a cylinder approximately 4 mm in diameter and 3 cm long with the axis oriented closely along the [1 1 0] axis. The structure exhibits only minimal orthorhombic distortion, and therefore scans were indexed in cubic geometry with a lattice parameter $a_0 = 3.84$ Å at 11 K.

The neutron measurements were made at the 10 MW University of Missouri Research Reactor utilizing the TRIAX triple-axis spectrometer. Below energy transfers of about 16 meV, a pyrolitic graphite (PG) monochromater and a PG analyzer at fixed final energy $E_f = 14.2$ meV were used with 80-40-S-40-40 Soller collimation (tighter collimation was used for some of the lower energy data.) Above 16 meV, a (2 2 0) pressed Cu monochromator and a PG analyzer fixed at $E_f = 14.2$ or 28 meV were used with 80-80-S-80-80 collimation. Graphite filters were used in the scattered beam position in all cases to suppress higher order contamination.

Inelastic neutron scattering data were taken along the $[q, q, q]$, $[q, q, 0]$, and $[0, 0, q]$ propagation directions at several temperatures between $T = 9$ K and $T_C = 273$ K. Both constant q and constant E scans were employed to optimize resolution and intensity. Excitations we ascribe to Mn–Mn exchange interactions, Nd–Mn exchange, optical phonons, and to the 11.8 meV crystal field level of the Nd ion were found in all three directions. We do not comment on the energy broadening of the magnon peaks near the zone boundary (as done in Ref. [17]), as apparent intersections of modes, and the statistical quality of our data prevent a reliable quantitative assessment of broadening as a function of q. For each of the measured Mn–Mn and Nd–Mn magnon modes, the low-q energy dispersion was fitted to the Heisenberg nearest-neighbor exchange model described in Eqs. (1) and (2). Significant departures from this model were observed at high q, as will be discussed later.

2.1. Mn–Mn modes

The measured excitation energies (excluding those ascribed to Nd–Mn modes) as a function of q (in relative lattice units) along the $[q, q, q]$, $[q, q, 0]$, and $[0, 0, q]$ propagation directions measured at 9 or 13 K are shown in Fig. 1. The solid lines are the fit of the Mn–Mn magnon dispersion from the fit to the Heisenberg nearest-neighbor exchange model. The zone boundary calculated energies

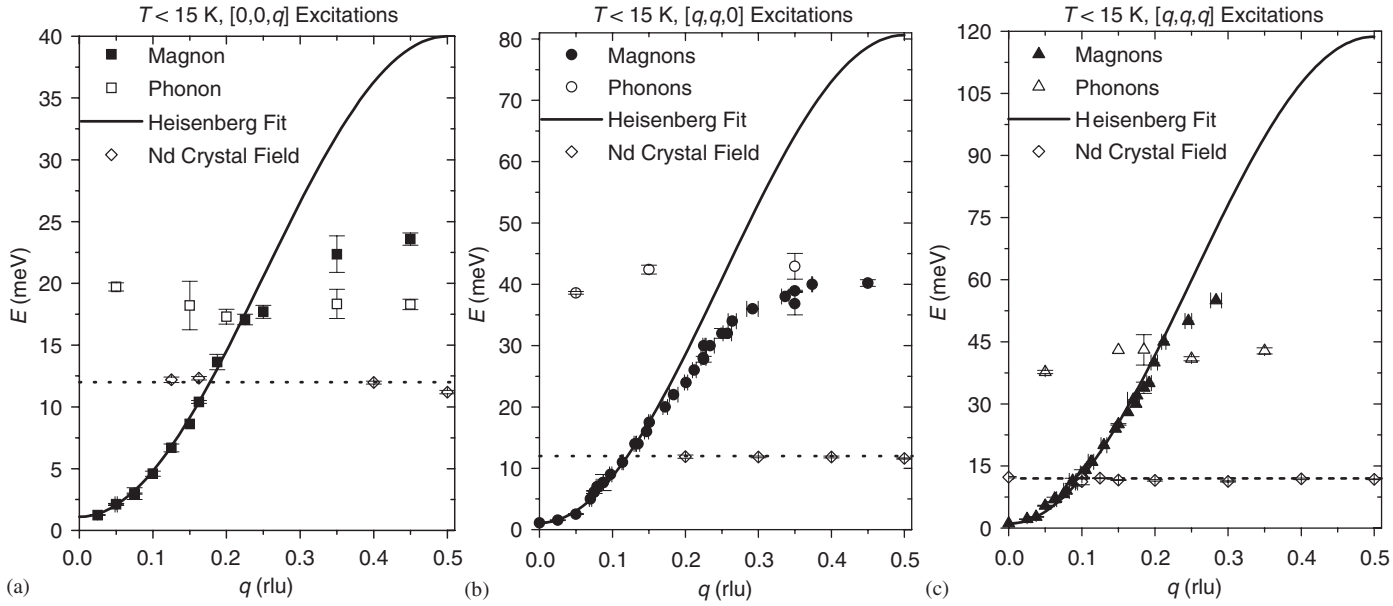

Fig. 1. Low-temperature excitation dispersions, featuring modes ascribed to the Nd crystal field, Mn–Mn magnon modes, and optical phonon modes. The low-q magnon data have been fitted to calculate Heisenberg nearest-neighbor model dispersions.

for the $[0,0,q]$, $[q,q,0]$, and $[q,q,q]$ modes found from the independent fits are 40, 80, and 112 meV, respectively, which are close to the expected 1:2:3 ratios. The dispersionless mode at 11.8 meV is the crystal field level of the Nd ion.

While the Heisenberg nearest-neighbor model accurately represents the Mn–Mn magnon modes at low q, above $q \approx 0.15$ rlu the modes in all three directions soften and depart from the calculated exchange. Additionally, in all three directions at low q, there are observed excitations at energies above those of the corresponding calculated Heisenberg dispersion. Since it is unlikely that the magnon modes would suddenly and drastically *stiffen*, we suggest that excitations that fall to the left of the calculated dispersions in Fig. 1 are optical phonons. As stated above, Dai et al. [18] detected magnon mode softening in the $[0\,0\,q]$ and $[q\,q\,0]$ directions for a $NdSrMnO_3$ sample of higher Nd concentration, and attributed that softening to interaction with optical phonon modes at about 20 and 40 meV, respectively. We see similar results for the $[0\,0\,q]$ and $[q\,q\,0]$ directions in the present study. Panels a and b of Fig. 2 show constant q energy scans at selected wave vectors in the $[0\,0\,q]$ and $[q\,q\,0]$ directions that show the suggested magnon–phonon interactions. The solid lines are Gaussian fits to the inelastic scattering data. Fig. 2a shows scans around 20 meV in the $[0\,0\,q]$ direction. The upward tailing action on the low-energy side of these scans is due to interference from the intense Nd ion crystal field level at 11.8 meV. In Fig. 2a, likely phonon excitations are shown at $q = 0.05$ and 0.15 rlu. The excitation at $q = 0.25$ rlu is likely to be a magnon, as it lies along the calculated Mn–Mn dispersion. Despite careful measurements, no evidence could be found of excitations at higher energies along the calculated dispersion in the $[0\,0\,q]$ direction. However, Fig. 2a shows excitations departing from the calculated dispersion, at $q = 0.35$ and 0.45 rlu, each with a dual peak character. This again suggests a softening of the $[0\,0\,q]$ Mn–Mn magnon mode upon intersection with a 20 meV optical phonon, possibly resulting in a mixed mode. This is displayed in Fig. 1a (note that in Fig. 1, these possible mixed modes are represented as a magnon and a phonon at the same q value, but differing in energy—but it is not completely clear which mode is which). Fig. 2b shows constant-q energy scans around 40 meV in the $[q\,q\,0]$ direction, that tell a similar story to those from Fig. 2a. Again, likely phonons are seen at $q = 0.05$ and 0.15 rlu. At $q = 0.25$ rlu the left side of the scan shows what is probably a magnon that has already softened from the calculated dispersion, and on the right appears an excitation that could be part of the optical phonon mode. Again, higher energy scans along the calculated $[q\,q\,0]$ Mn–Mn magnon dispersion revealed no further excitations. At $q = 0.35$ rlu, Fig. 2b shows an excitation with dual peak character, and at $q = 0.45$ rlu, a very broad, unresolved excitation that could be the result of a mixed magnon and phonon. So, by examining Figs. 1b and 2b, it appears that for the $[q\,q\,0]$ direction, the Mn–Mn magnon mode begins to soften at $E \approx 20$ meV, and then becomes unobservable at higher energies, upon intersection with an optical phonon mode at $E \approx 40$ meV.

For the $[q\,q\,q]$ direction (unexamined in Refs. [15,17] for $NdSrMnO_3$), the Mn–Mn magnon dispersion again appeared to intersect with a phonon branch, but with somewhat different results than in the other two directions. Fig. 2c shows constant q scans around $E = 40$ meV in the $[q\,q\,q]$ direction. Apparent phonons are again observed, at $q = 0.05$ and 0.15 rlu. At $q = 0.185$ rlu, a probable magnon is visible on the left, with an energy falling on the calculated

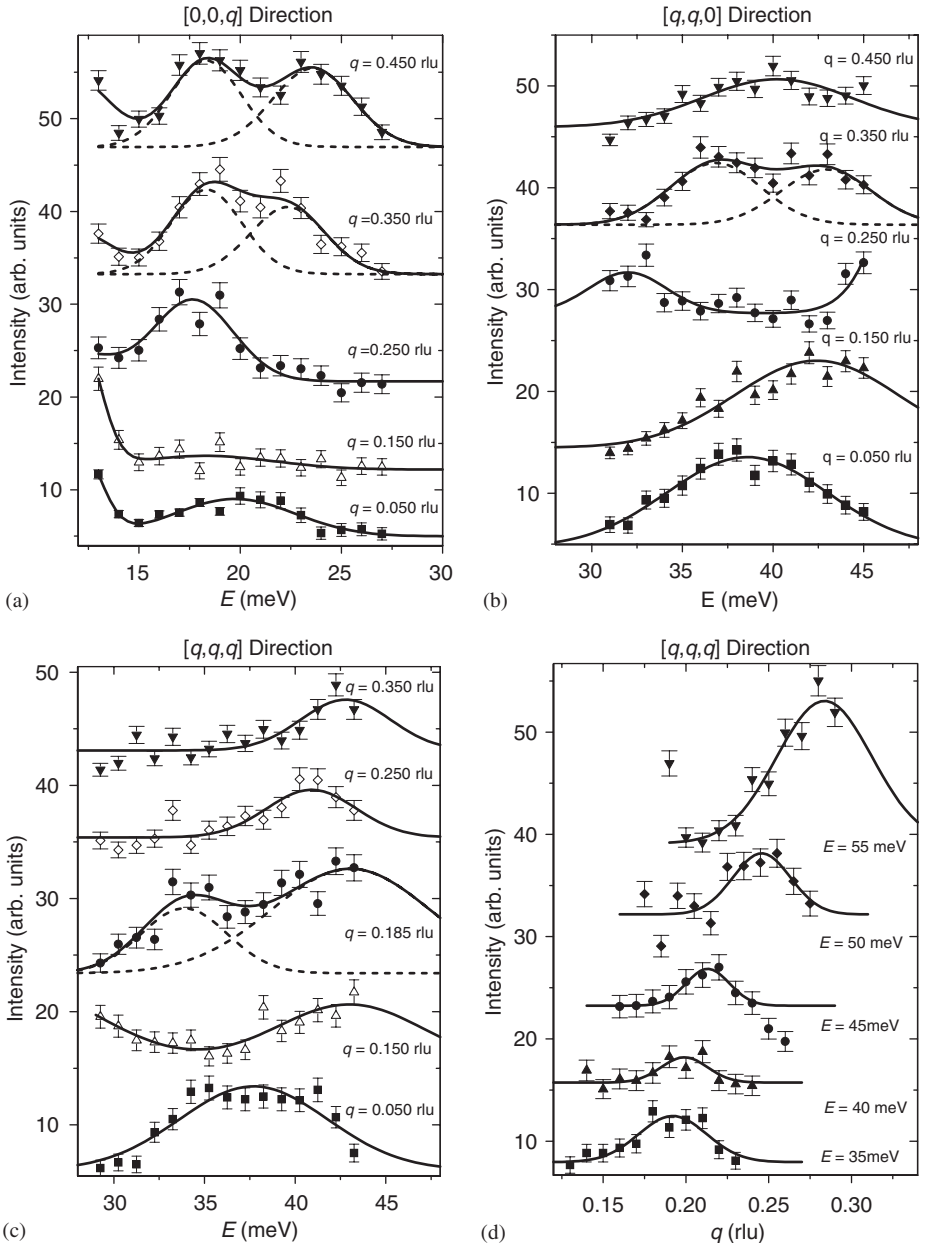

Fig. 2. Inelastic neutron scattering data showing the intersection of modes ascribed to Mn–Mn magnons and optical phonons.

dispersion curve, and what is likely to be a phonon is visible on the right. Excitations that appear to consist of single peaks are shown at $q = 0.25$ and 0.35 rlu. What is different from the cases of the [0 0 q] and [q q 0] directions is that higher energy scans along the calculated magnon dispersion do reveal excitations at energies above the apparent phonon–magnon intersection, suggesting that the $q = 0.25$ and 0.35 rlu excitations in Fig. 2c are not mixed mode excitations, but only phonons. These higher energy excitations are shown in Fig. 2d, which is a series of q scans at constant E, at q values near those of the calculated dispersion. Fig. 2d shows excitations at 35, 40, and 45 meV that follow the calculated dispersion. Excitations are also visible at 50 and 55 meV, which show signs of softening with respect to the calculated dispersion. Considering Figs. 1c, 2c, and d, the data suggest that the [q q q] Mn–Mn magnon mode intersects an optical phonon mode at $E \approx 40$ meV, but that the magnon mode does not abruptly soften, instead continuing on to higher energy, with a gradual softening. Pursuit of excitations at higher energies was not practical, due to instrumental limits.

3. Spin stiffness

Measurements of the low-q Mn–Mn magnon modes were taken at a series of temperatures, and fitted using Eq. (2), in order to determine the temperature renormalization of the spin stiffness parameter D. At $T = 13$ K, the fits

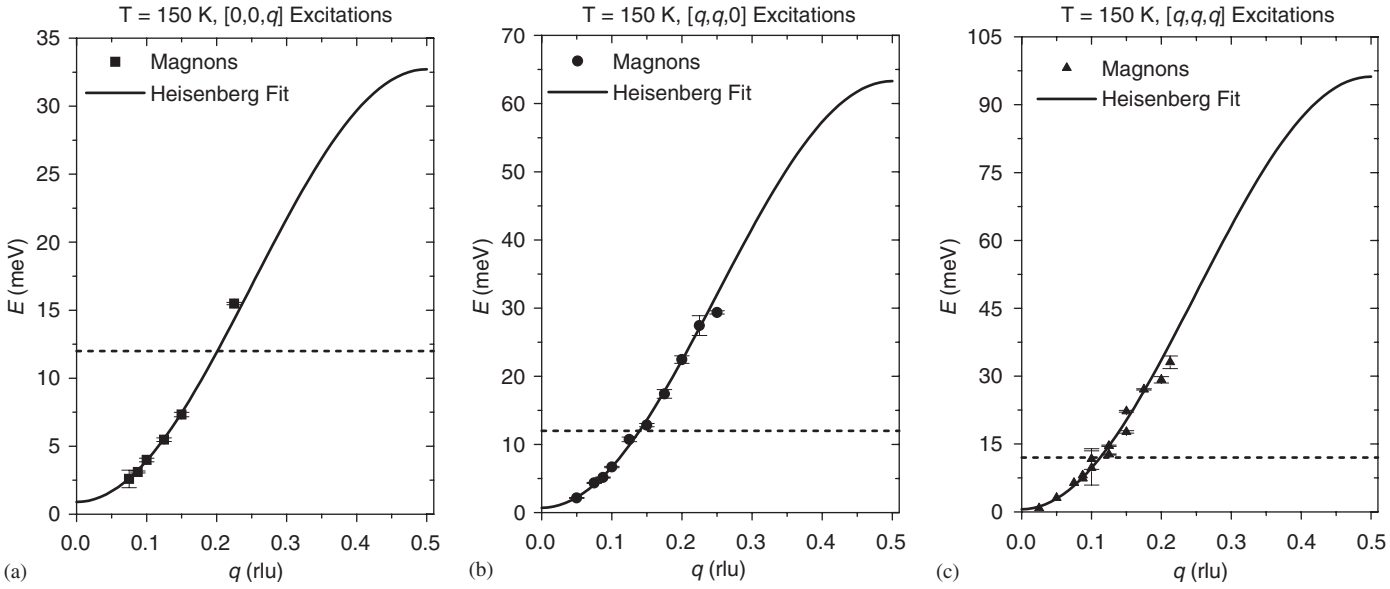

Fig. 3. Dispersion of modes ascribed to Mn–Mn magnons at $T = 150\,\mathrm{K}$.

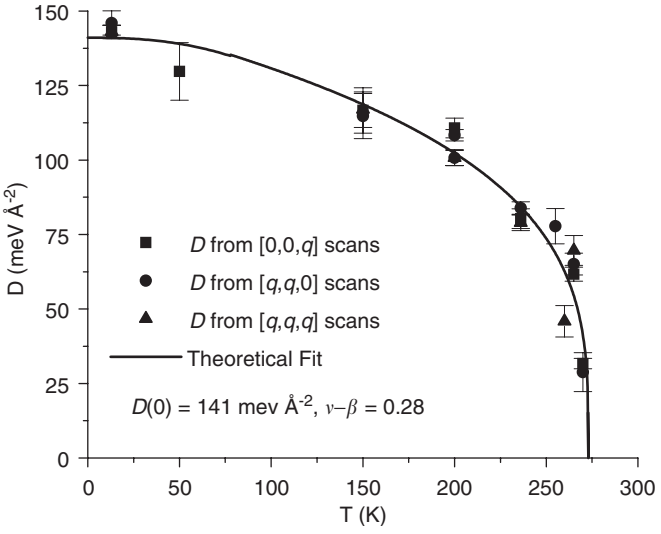

Fig. 4. Temperature dependence of the Mn–Mn magnon spin stiffness.

produced values of D equal to 143, 146, and 143 meV Å^2 in the $[q\,q\,q]$, $[q\,q\,0]$, and $[0\,0\,q]$ directions, respectively, indicating isotropic behavior as expected. The $q = 0$ rlu energy gap was 1.1 meV, a value somewhat larger than in other manganites with only a single magnetic ion (Mn), and is ascribed to the Nd spin dynamics and anisotropy discussed below.

As an example of the higher temperature data, Fig. 3 shows the Mn–Mn magnon dispersions in the $[0\,0\,q]$, $[q\,q\,0]$, and $[q\,q\,q]$ directions at $T = 150\,\mathrm{K}$. The dashed line in Fig. 3 represents the Nd ion crystal field level. The zone boundary calculated energies for the $[0\,0\,q]$, $[q\,q\,0]$, and $[q\,q\,q]$ modes were found to be 33, 63, and 96 meV, respectively, close to the expected 1:2:3 ratios as was the case at $T = 13\,\mathrm{K}$. However, the energies themselves are smaller than those at $T = 13\,\mathrm{K}$, indicative of reduced spin stiffness—which at $T = 150\,\mathrm{K}$ was found to be 117, 115, and 117 meV Å^2 in the $[q\,q\,q]$, $[q\,q\,0]$, and $[0\,0\,q]$ directions, respectively. The temperature dependence of the magnon stiffness parameters is shown in Fig. 4, derived from fits to dispersion data for all three propagation directions. The low T (13 and 50 K) spin stiffness data points were fit using the $T^{5/2}$ model from Eq. (3). This fit yields $D(0) = 141\,\mathrm{meV\,Å^{-2}}$, a normal value for a manganite. The remaining higher T spin-stiffness data points are fit using the power-law model from Eq. (4). This fit shows that the temperature renormalization of D is conventional for a second-order phase transition, with D approaching zero at T_C with $\nu - \beta = 0.27$, somewhat below the standard Heisenberg value. There is no evidence of a discontinuity in D as $T \to T_C$, in contrast to $La_{0.7}Ca_{0.3}MnO_3$ and $Nd_{0.7}Sr_{0.3}MnO_3$.

3.1. Nd–Mn modes

Magnon data taken at the lowest temperatures show the existence of a second set of dispersive modes as exhibited in Fig. 5 (reproduced from Ref. [20]). These additional branches are ascribed to modes involving the Nd spins via Nd–Mn exchange coupling. The solid lines are Heisenberg nearest-neighbor fits to the data. The Nd–Mn and Mn–Mn modes appear to merge with each other, and with the crystal field level at larger q. An example of this can be seen in Fig. 6, which shows a series of constant-q energy scans at selected wave vectors in the $[q\,q\,0]$ direction. Fig. 6 shows that for both the $q = 0.025$ and 0.05 rlu scans, two excitations are visible:the left one ascribed to the Mn–Mn mode and the right one ascribed to the Nd–Mn mode. For $q = 0.075$ and 0.0875 rlu, the two modes seem to

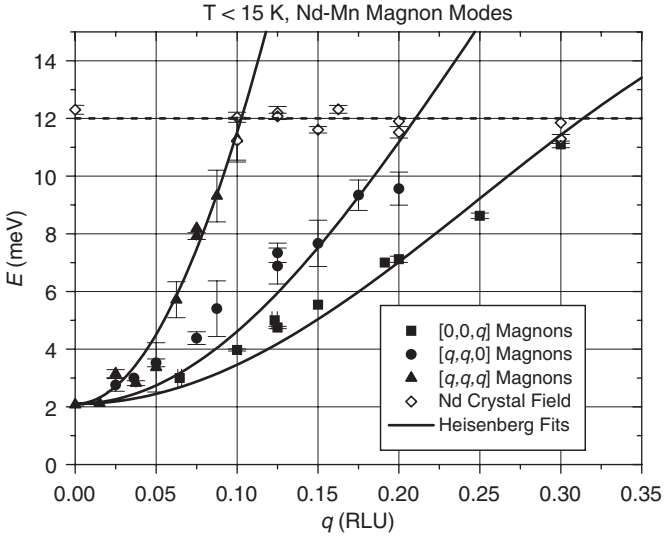

Fig. 5. Dispersion of excitation modes attributed to Nd–Mn magnons (from Ref. [20]).

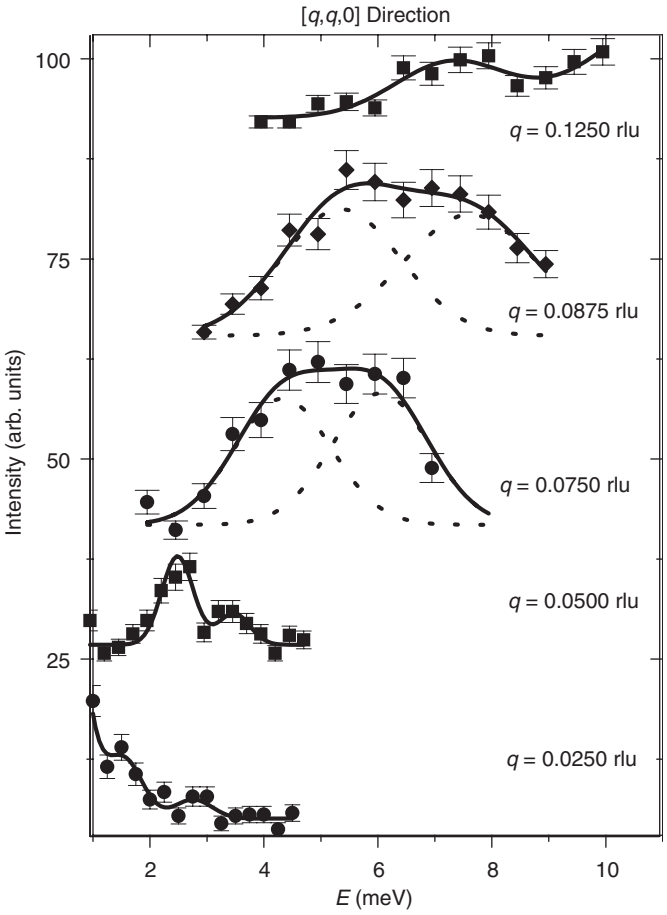

Fig. 6. Inelastic neutron scattering data showing the intersection of modes ascribed to Mn–Mn and Nd–Mn magnons.

have merged together. At $q = 0.125$ rlu, the two modes appear to have crossed completely, as only one excitation remains—likely part of the Mn–Nd mode. A careful search along $[0\,0\,q]$ revealed no excitations at higher energies.

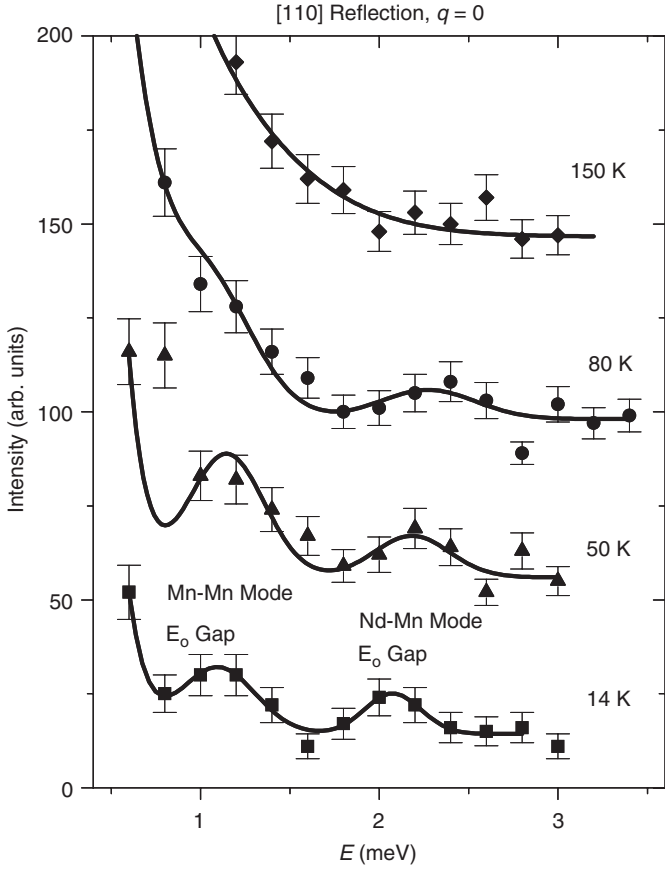

Fig. 7. Low energy, $q = 0$ rlu inelastic neutron scattering data illustrating the different energy gaps for the Mn–Mn and Nd–Mn magnon modes.

When plotted in absolute q (Å^{-1}) the $[q\,q\,0]$ and $[0\,0\,q]$ modes are isotropic; however the $[q\,q\,q]$ branch has somewhat higher dispersion and closely parallels the Mn–Mn $[q\,q\,q]$ branch, suggesting some admixture of these modes may be occurring. As further evidence that the modes ascribed to Mn–Mn and Nd–Mn interactions are independent, the $q = 0$ rlu energy gaps were measured as functions of temperature, as shown in Fig. 7. At 14 K, the Nd–Mn modes exhibit a $q = 0$ rlu gap of 2.2 meV, nearly twice as large as that for the Mn–Mn mode. The larger 2.2 meV gap is consistent with the magnitude of the Nd single ion anisotropy.

4. Conclusion

In summary, inelastic magnetic neutron scattering has been used to examine the magnon dispersions for $Nd_{0.6}Sr_{0.4}MnO_3$ in the $[0\,0\,q]$, $[q\,q\,0]$, and $[q\,q\,q]$ directions. In all three directions, the dispersions showed significant softening as compared to a Heisenberg nearest-neighbor model, as has been seen in other CMR manganites [9,14–17]. The temperature renormalization of the spin stiffness was shown to correspond to a second-order phase transition, but with a power-law exponent lower than that

expected for a Heisenberg ferromagnet. Additionally, separate magnetic modes in all three directions were found, and attributed to the Nd–Mn exchange interaction.

References

[1] R. von Helmot, B. Holzapfel, I. Schultz, K. Samwer, Phys. Rev. Lett. 63 (1993) 1990.
[2] S.H. Jin, T.H. Tiefel, M. McCormack, R.A. Fastnacht, R. Ramesh, L.H. Chen, Science 264 (1994) 413.
[3] C. Zener, Phys. Rev. 118 (1951) 403.
[4] J.B. Goodenough, Prog. Solid State Chem. 5 (1971) 149.
[5] P.G. DeGennes, Phys. Rev. 118 (1960) 141.
[6] A.J. Millis, Nature 392 (1998) 147.
[7] P. Dai, J. Zhang, H.A. Mook, S.-H. Liou, P.A. Dowben, E.W. Plummer, Phys. Rev. B 54 (1996) R3694.
[8] P.G. Radaelli, D.E. Cox, M. Marezio, S.-W. Cheong, B. Battlog, Phys. Rev. B 54 (1996) 8992.
[9] S.J.L. Billinge, R.G. DiFrancesco, G.H. Kwei, J.J. Neumeier, J.D. Thompson, Phys. Rev. Lett. 77 (1996) 715.
[10] P. Dai, J.A. Fernandez-Baca, N. Wakabayashi, E.W. Plummer, Y. Tomioka, Y. Tokura, Phys. Rev. Lett. 85 (2000) 2553.
[11] C.P. Adams, J.W. Lynn, Y.M. Mukovskii, A.A. Arsenov, D.A. Shulyatev, Phys. Rev. Lett. 85 (2000) 3954.
[12] Jiandi Zhang, P. Dai, J.A. Fernandez-Baca, E.W. Plummer, Y. Tomioka, Y. Tokura, Phys. Rev. Lett. 86 (2001) 3823.
[13] T.G. Perring, G. Apelli, S.M. Hayden, S.A. Carter, J.P. Remeika, S.W. Cheong, Phys. Rev. Lett. 77 (1996) 711.
[14] M.C. Martin, G. Shirane, Y. Endoh, K. Hirota, Y. Moritomo, Y. Tokura, Phys. Rev. B 53 (1996) R14285.
[15] J.A. Fernandez-Baca, P. Dai, H.Y. Hwang, C. Kloc, S.-W. Cheong, Phys. Rev. Lett. 80 (1998) 4012.
[16] H.Y. Hwang, P. Dai, S.-W. Cheong, G. Aeppli, D.A. Tennant, H.A. Mook, Phys. Rev. Lett. 80 (1998) 1316.
[17] P. Dai, H.Y. Hwang, Jiandi Zhang, J. A. Fernandez-Baca, S.-W. Cheong, C. Kloc, Y. Tomioka, Y. Tokura, Phys. Rev. B 61 (2000) 9553.
[18] L.M. Woods, Phys. Rev. B 65 (2001) 014409.
[19] T.A. Kaplan, S.D. Mahanti, J. Phys.: Condens. Matter 9 (1997) L291.
[20] H. Kaiser, L.E. Stumpe, J.J. Rhyne, Y. Tokura, H. Kuwahara, J. Appl. Phys. 85 (1999) 5564.